Crossover Sorption of C_2H_2/CO_2 and C_2H_6/C_2H_4 in Soft Porous Coordination Networks

Mohana Shivanna,[a] Ken-ichi Otake,[a]* Shotaro Hiraide,[b]* Takao Fujikawa,[a] Ping wang,[a] Yifan Gu,[a] Hirotaka Ashitani,[c,d] Shogo Kawaguchi,[d] Yoshiki Kubota,[c,e] Minoru T. Miyahara,[b] and Susumu Kitagawa[a]*

[a] Institute for Integrated Cell-Material Sciences, Kyoto University Institute for Advanced Study, Kyoto University, Yoshida Ushinomiya-cho, Sakyo-ku, Kyoto 606-8501, Japan.
  Email: ootake.kenichi.8a@kyoto-u.ac.jp; kitagawa@icems.kyoto-u.ac.jp
[b] Department of Chemical Engineering, Kyoto University, Nishikyo, Kyoto 615-8510, Japan.
  Email: hiraide@cheme.kyoto-u.ac.jp
[c] Department of Physical Science, Graduate School of Science, Osaka Prefecture, University, Sakai, Osaka 599-8531, Japan.
[d] Japan Synchrotron Radiation Research Institute (JASRI), SPring-8, 1-1-1 Kouto, Sayo-cho, Sayo-gun, Hyogo 679-5198, Japan.
[e] Department of Physics, Graduate School of Science, Osaka Metropolitan University, Sakai, Osaka 599-8531, Japan.
  Supporting information for this article is given via a link at the end of the document.

Abstract: Porous sorbents are materials that are used for various applications, including storage and separation. Typically, the uptake of a single gas by a sorbent decreases with temperature, but the relative affinity for two similar gases does not change. However, in this study, we report a rare example of "crossover sorption," in which the uptake capacity and apparent affinity for two similar gases reverse at different temperatures. We synthesized two soft porous coordination polymers (PCPs), $[Zn_2(L1)(L2)_2]_n$ (PCP-1) and $[Zn_2(L1)(L3)_2]_n$ (PCP-2) (L1= 4,4'-bis(4-pyridyl) phenyl, L2= 5-methyl-1,3-di(4-carboxyphenyl)benzene, and L3= 5-methoxy-1,3-di(4-carboxyphenyl)benzene). These PCPs exhibits structural changes upon gas sorption and show the crossover sorption for both C_2H_2/CO_2 and C_2H_6/C_2H_4, in which the apparent affinity reverse with temperature. We used in-situ gas-loading single-crystal X-ray diffraction (SCXRD) analysis to reveal the guest inclusion structures of PCP-1 for C_2H_2, CO_2, C_2H_6, and C_2H_4 gases at various temperatures. Interestingly, we observed three-step single-crystal to single-crystal (sc-sc) transformations with the different loading phases under these gases, providing insight into guest binding positions, nature of host-guest or guest-guest interactions, and their phase transformations upon exposure to these gases. Combining with theoretical investigation, we have fully elucidated the crossover sorption in the flexible coordination networks, which involves a reversal of apparent affinity and uptake of similar gases at different temperatures. We discovered that this behaviour can be explained by the delicate balance between guest binding and host-guest and guest-guest interactions.

Introduction

The adsorption process using porous sorbents is an attractive method for separating similar guest species and has the potential to improve upon traditional separation methods. Conventional porous sorbents such as zeolites or carbon-based materials have been well studied for storage or separations and other applications.[1] However, their lack of tunability limits their performance and their ability to targets specific applications. A new class of porous materials called porous coordination polymers (PCPs)[2] or metal-organic frameworks (MOFs),[3] are a subclass of porous materials that consists of both organic and inorganic components, and exhibits extraordinary diversity in composition. These crystalline porous materials have been classified into three "generations" based upon their structural features:[4] 1st generation materials are capable of accommodating guest molecules but their removal results in the decomposition of the network; 2nd generation or rigid materials retain their original structure upon guest insertion/removal and exhibit a "permanent porosity"; 3rd generation materials, also termed as flexible MOFs or soft PCPs, show reversible structural transformations upon exposure to stimuli such as heat, gas/vapor or light.[4b, 5] Typically, soft PCPs exhibit "stepped" or "S-shaped" isotherm when they expose to single component gases, while rigid sorbents typically follow a type-I sorption profile.[6] When two similar gases are present

under a constant pressure, sorbents tend to show an increase in uptake for gases as the temperature decreases, while maintaining the same relative affinity between the two gases (Figure 1a).[7] This is because the order of adsorption energy for a given gas-adsorbent system remains relatively constant across a wide range of temperatures. However, in this study, we report on a rare occurrence of "crossover sorption," in which the uptake capacity and apparent affinity for two similar gases reverse at different temperatures (Figure 1b). This behaviour could potentially result in switching the selectivity of one gas species over another with varying temperatures. Therefore, sorbents that exhibits crossover phenomena could eliminate the need for using two separate sorbents for selectively separating a single gas component from a mixture gases like C_2H_2/CO_2 and CO_2/C_2H_2, as well as other industrially important gases. It is important to note that understanding such a unique system can uncover new mechanisms that can be utilized in designing new sorbents with enhanced performances in sorption-related applications. So far, there have been a few cases reported where the sorbent's apparent affinity toward gases reverses in temperature.[8] For example, the reversal in IAST selectivity was observed for sorption between at room temperature and at cryogenic temperatures for CO_2/C_2H_2 selectivity in [Mn(bdc)/(dpe)][9] and SIFSIX-23-Cu.[10] Similarly, Cu(Qc)$_2$ sorbent has been reported to show the different affinity toward C_2H_6/C_2H_4 gases at different temperature conditions.[11] However, there has been no detailed discussion or investigations into the origin of the inversed affinity of different gases in the PCPs under the different temperature condition.

Herein we synthesized two new soft PCPs, $[Zn_2(L1)(L2)_2]n$ (PCP-1) and $[Zn_2(L1)(L3)_2]n$ (PCP-2) (L1= 4,4'-bis(4-pyridyl) phenyl, L2= 5-methyl-1,3-di(4-carboxyphenyl)benzene, and L3= 5-methoxy-1,3-di(4-carboxyphenyl)benzene), which undergo structural transformation into the activated phase upon removal of guest molecules (Figure 1c-e). When the activated phases were exposed to C_2H_2, C_2H_4, C_2H_6, and CO_2 gases (Table S1), a stepped sorption behaviours were observed. Curiously, both PCP-1 and PCP-2 showed crossover sorption, in which the selectivities were reversed for pairs of similar gases, CO_2/C_2H_2 and C_2H_4/C_2H_6 (Figure 1b). To uncover the origin of this phenomenon, we studied the gas adsorption process using in-situ gas loading single-crystal x-ray diffraction (SCXRD) measurements at different temperatures. Additionally, we conducted density functional theory (DFT) calculations and free energy analysis with the aid of grand canonical Monte Carlo (GCMC) simulations to elucidate the mechanism. This is the first example of the full elucidation of the crossover sorption in flexible coordination networks, which displays a reversal of apparent affinity and uptake of similar gases at varying temperatures. We discovered that this behaviour can
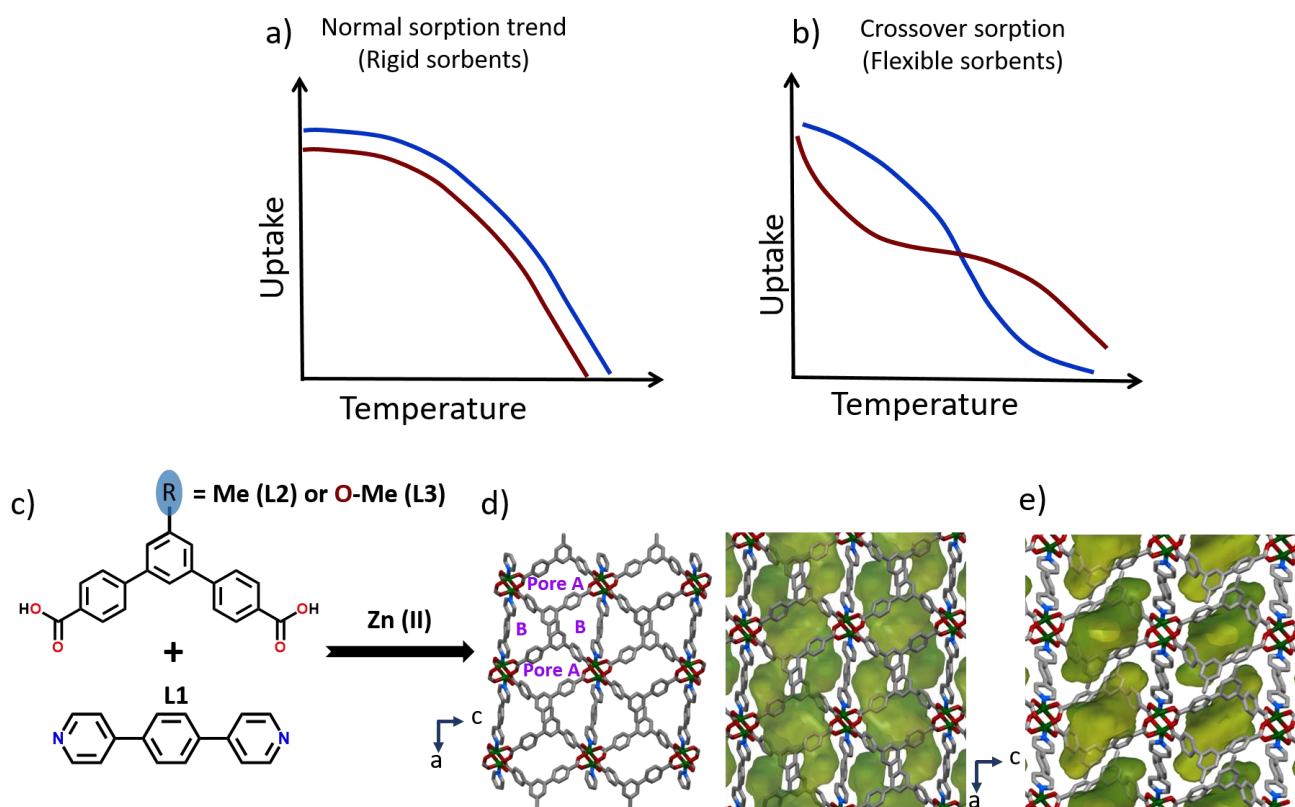
Figure 1. Types of sorption trend and structural representation. a) Rigid sorbents typically exhibit normal sorption trend for two similar gas species, while b) Flexible sorbent exhibits crossover sorption with change in uptake capacity and apparent affinity while varying temperature. c) Chemical structure of organic linkers 5-methyl (or methoxy)-1,3-di(4-carboxyphenyl)benzene, 4,4'-bis(4-pyridyl)biphenyl and inorganic component, Zn(II). d) These components form a 3D network as viewed the closed packed structure and guest accessible channels along the b-axis. e) The as-synthesised phase undergoes structural transformation upon heating lead to reduction in void space and obtain one dimensional channels as shown for the activated phase.

be explained by the delicate balance between guest binding and host-guest and guest-guest interactions.

Results and Discussion

Single crystals of PCP-1 and PCP-2 were synthesized[12] from the solvothermal reactions using N,N-Dimethylformamide (DMF) solvent at 100 °C for 2 days (Figure S1-5, see supporting information). SCXRD analysis showed that both as-synthesized phases of PCP-1 and PCP-2 (hereafter referred to as the α structure) form 3D networks with Zn paddle wheel secondary building units (SBUs), in which L1 coordinated along the axial position and L2 or L3 is placed in the equatorial positions. The α structures of PCP-1 and PCP-2 both crystallize in the monoclinic *C2/c* space group (Table S2 and S3), with 29% and 28% of the guest accessible channels being occupied by solvent molecules, respectively. Topos analysis determined that the frameworks belong to a rare type 6-connected net, $4^4 \cdot 6^{10} \cdot 8$ topology (6T9 type). Single crystals of the activated phases[12] were obtained by heating the as-synthesized phase above 120 °C for ~12 h (supporting information). Upon activation, crystals retained the same space group, but there were notable changes in the unit cell parameters (Table S2 and S3). The crystal structure analysis revealed that 3D networks were distorted, and the guest-accessible volume was reduced to 20% (PCP-1) and 22% (PCP-2) (hereafter referred to as the β structure). The square paddlewheel nodes underwent slight contortion during the transformation from the as-synthesized phase to the activated phase, as shown in Figure S6. Regarding the L1, L2 or L3 linkers, large distortions were observed for PCP-1 in the as-synthesized phase, with ∠L1-SBU-L2 = 67.94°–113.94°, and in the activated phase, ∠L1-SBU-L2 = 63.68°–116.34° as shown in Figure S7. Similarly, in for

PCP-2, the angle changed from ∠L1-SBU-L3 = 74.89° –105.10° in the as-synthesized phase to ∠L1-SBU-L3 = 62.83°–118.93° upon activation. We also observed significant changes in the pore size, from 7.12 to 6.36 Å for pore A in PCP-1 and from 7.12 to 6.36 Å at pore A in PCP-2. Additionally, the pore environments at pore B were affected by the movement of methyl functionality (from 5.26 to 6.86 Å) in PCP-1 and methoxy functionality (5.26 to 6.86 Å) in PCP-2 (Figure S1-2 and S4-5). Thermogravimetric analysis (TGA) indicated that PCP-1 and PCP-2 were stable up to above 300 °C for as-synthesized and activated samples (Figure S8-9).

To evaluate the gas sorption performance of the obtained PCPs, we first measured the CO_2 and C_2H_2 sorption isotherms for PCP-1 at different temperatures (Figure 2a and Figure S10-14). We found that the C_2H_2 exhibited a typical type-I isotherm at 195 K, with a slight inflection at low pressure followed by a gradual increase in uptake (160 cm³/g) up to the highest pressure we tested (~100 kPa). The CO_2 sorption curve, on the other hand, had a small plateau at the low pressure (< 10 kPa) with an uptake of up to 110 cm³/g, followed by a step leading to an uptake of 180 cm³/g at 100 kPa. When tested at higher temperatures, we found that CO_2 sorption followed a type-I sorption profile with uptakes of 60 and 80 cm³/g at 298 K and 273 K, respectively (Figure 2b and S13). C_2H_2 had a gate opening at 60 and 20 kPa at these temperatures, with saturated uptakes of 80 and 100 cm³/g, respectively. These sorption isotherms showed that C_2H_2 had higher uptake at 298 K and 273 K (Figure 2b and S13), but lower uptake at 195 K compared to CO_2. To further investigate these inverse behaviours at different temperatures, we conducted the sorption isobar measurements under a constant gas pressure of 100 kPa (Figure 2c). We found that at 195 K, CO_2 had higher uptake than C_2H_2 by 18 cm³/g. However, as the temperature increased to 230 K, both gases' uptakes

2

crossed over, and when we further lowered the temperature to 298 K, CO_2 uptake became lower than C_2H_2. We also observed an inflection at around 240 K followed by a sudden drop in uptake from 125 to 100 cm^3/g. In the C_2H_2 isobar, we noticed a continuous decrease in uptake up to the gate closing temperature of 310 K (40 cm^3/g). Similar trends were observed during the cooling process (Figure S14), except for a small difference in the gate opening temperatures. These isobar sorption measurements were consistent with the isotherm measurement results.

Such unusual crossover sorption motivated us to investigate other gases such as C_2H_6 and C_2H_4 (Figure S15-18). We found that at 170 K for C_2H_4 and 185 K for C_2H_6 (Figure 2d), both gases exhibited similar sorption trends at low pressure, up to 0.1 kPa, followed by a small inflection point when the uptake reached 40 cm^3/g. However, as we increased the pressure, there were significant differences in the uptake and affinity between the two gases. C_2H_4 had a saturation uptake of 140 cm^3/g, whereas C_2H_6 had a saturation uptake of 120 cm^3/g at approximately 100 kPa (Figure 2d and S15). To further investigate the apparent affinity change, we conducted sorption measurements at the same temperature (185 K) for both gases. Our results (Figure S15) indicate that at low pressure, gate opening occurred first for C_2H_6 (<0.04 kPa) before C_2H_4 (<0.1 kPa) when the uptake reached around 40 cm^3/g. With a further increase in pressure, the gate opening profiles switched, with C_2H_4 opening earlier (0.9 kPa) than C_2H_6 (over 10 kPa). At a temperature of 298 K, we observed that C_2H_6 sorption showed a step at 75 kPa before reaching a saturated pressure of approximately 100 kPa (65 cm^3/g, as shown in Figure 2e). In contrast, for C_2H_4 sorption, there were no steps, and we observed a typical type-I isotherm with an uptake capacity of 40 cm^3/g at around 100 kPa, which was less than the uptake of C_2H_6 (Figure 2e). At 273 K, both gases showed stepped sorption; however, gate opening occurred earlier for C_2H_6 (20 kPa) than C_2H_4 (42 kPa), indicating that PCP-1 has a stronger affinity for C_2H_6 at

these temperature ranges (Figure S16). To our knowledge, there are only a few examples in the literature that demonstrate C_2H_6 preference over C_2H_4,[11, 13] but no examples have been reported for crossover type sorption with different temperatures. As shown in Figure 2f, the sorption isobar measurements at 100 kPa show that C_2H_4 has a higher uptake than C_2H_6 at low temperatures, and the crossover temperature was found to be at 268 K, consistent with the isotherm measurements. As the temperature increases, the uptake of C_2H_6 becomes higher than that of C_2H_4. We were able to reproduce the same sorption trends during the cooling process, with only a slight difference in the crossover temperature (263 K) and the gate opening temperatures, as shown in Figure S18.

PCP-2 exhibits the same crossover sorption behaviour as PCP-1 when exposed to C_2H_2/CO_2 and C_2H_6/C_2H_4 gases, as shown in Figure S19-25 and Table S4. Interestingly, the crossover temperature between C_2H_2 and CO_2 was found to be 255 K, whether the gases were heated or cooled. Meanwhile, C_2H_6/C_2H_4 gases undergo crossover at 268 K and 273 K during heating and cooling, respectively. This temperature is 25 K higher for C_2H_2/CO_2 and 10 K higher for C_2H_6/C_2H_4 (cooling) compared to the crossover temperature observed for PCP-1. This difference is attributed to the methoxy functionalization in the L3 ligand. Thus, our findings suggest that tuning the crossover temperature can be achieved through functionalization with other groups, such as sulphur, nitro, alcohol, and others, which could be valuable for distinguishing similar guest species.

To ensure the phase purity of the guest inclusion structures of PCP-1, we used synchrotron diffraction to collect in-situ Powder X-ray diffraction (PXRD) data at various temperatures. The measured in-situ PXRD patterns matched the simulated patterns based on single-crystal structures, as shown in Figure S26-29. We also collected PXRD patterns at every adsorption/desorption point for C_2H_6 (185 K), C_2H_4 (170 K), C_2H_2 (195 K), and CO_2 (195 K) sorption to understand the structural transformations in detail (Figure S30-33). The initial loading pattern
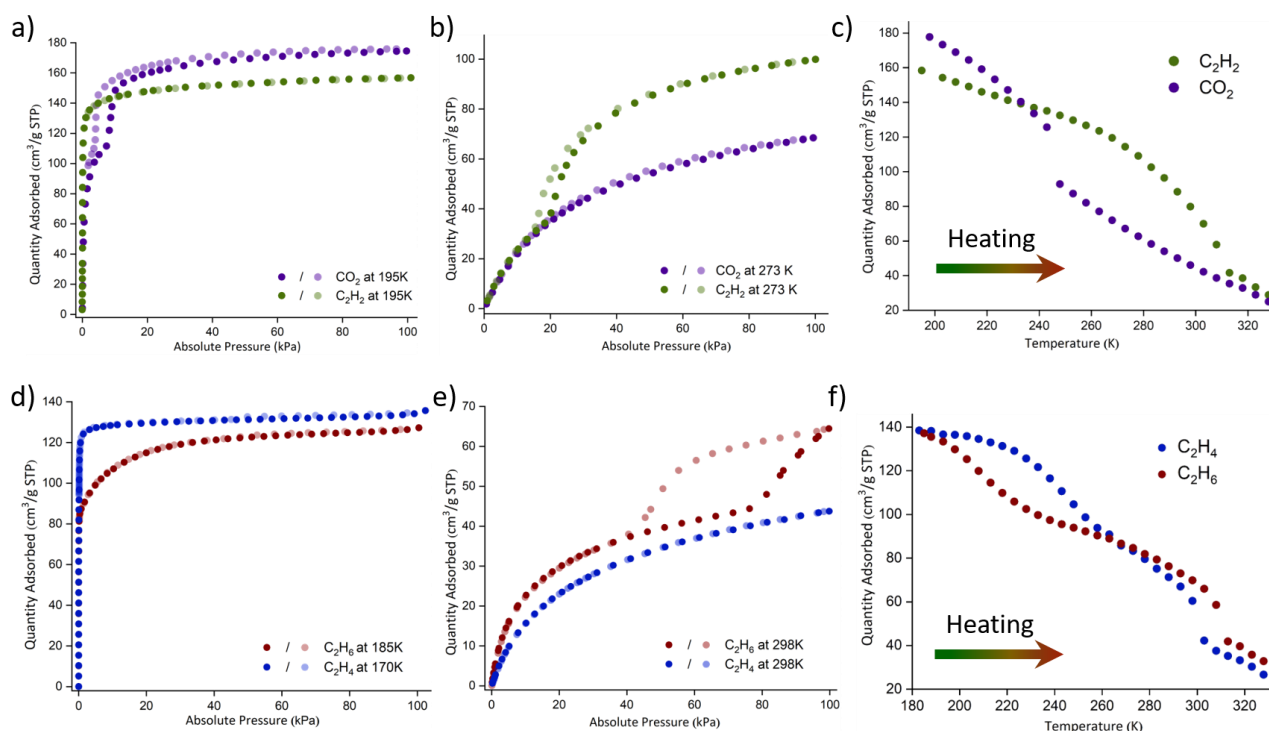

Figure 2. The single component and isobar measurements for PCP-1. a) and b) C_2H_2 and CO_2 sorption measured at 195 K and 273 K, respectively. c) C_2H_2 and CO_2 isobar measured while increase in the temperatures from low to high. d) C_2H_6 and C_2H_4 sorption isotherm measured at 185 K and 170 K, respectively. e) C_2H_6 and C_2H_4 sorption isotherm at 298 K. f) Isobar plot for C_2H_6 and C_2H_4 gases measured while increase in the temperatures from low to high.
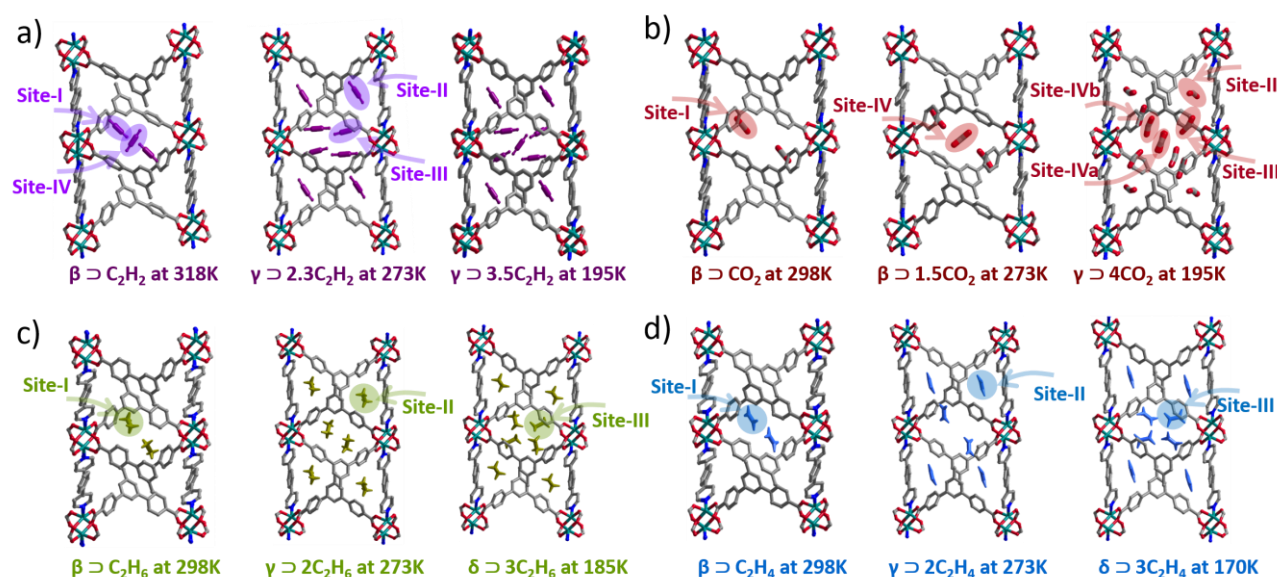
Figure 3. Structural representation of guest inclusion structures of PCP-1 from in-situ single crystal diffraction. a) Upon C_2H_2 dosing at 318 K, one C_2H_2 distributed between site-I and site-IV. At 273 K, 2.3C_2H_2 occupied at site-I, site-II and site-III positions. When temperature reached to 195 K, four sites (site-I, site-II, site-III and site-IV) filled with total 3.5 molecules. b) With respect to CO_2, one CO_2 filled at site-I (298 K), followed by 1.5CO_2 occupied at site-I and site-IV (273 K). At 195 K there are 4 CO_2 molecules occupied at five sites (site-I, site-II, site-III, site-IVa and site-IVb. c and d) C_2H_4 or C_2H_6 occupy at the site-I position at 298 K, while temperature decreased to 273 K the second C_2H_4 or C_2H_6 occupy at the site-II position. Then the site-III position filled by 3rd C_2H_4 or C_2H_6 at 170 and 185 K, respectively.

matched the calculated pattern of β⊃empty for all four gases. When the pressure increased slightly, a first-order phase transition occurred. At saturation points 26, 29, 29, and 52, the phases matched the calculated δ⊃3C_2H_6, δ⊃3C_2H_4, γ⊃3.5C_2H_2, and γ⊃4CO_2, respectively (*vide infra*). Furthermore, we investigated the structural changes of the activated β structure at various temperatures (Figure S34), clearly indicating that the variations in the β structure due to temperature changes are small. Additionally, we confirmed the sample's regenerability after sorption by treating it with heat at 40 °C for 1 hour under vacuum, as shown in Figure S35-36.

To uncover the origin of the crossover sorption, we investigated the gas adsorption process using in-situ gas loading single-crystal x-ray measurements under different temperatures in a snapshot-like fashion (Figure 3a-d Figure S37-S52). We determined the gas-adsorbed structures[12] of C_2H_2 and CO_2 under a gas pressure of ~100 kPa at four different temperatures: 318 K, 298 K, 273 K, and 195 K. As shown in Figure 3a and 3b, when exposed to CO_2 or C_2H_2 initially, the β⊃empty structure accommodates one guest species resulting in β⊃CO_2 at 298 K and β⊃C_2H_2 at 318 K. The β structure with guest molecules maintains almost the identical unit cell parameters to the empty β phase (Table S2). Interestingly, even though both guest species have the same amount, CO_2 occupies only one position (site-I) while C_2H_2 occupies two (site-I and site-IV) positions. In these structures, C_2H_2 engages in various types of host-guest interactions with the framework. For example, at site-I, it forms multiple σ···σ (C-H···H, $D_{C \cdots H}$ = 3.382, 3.600, and 3.824 Å) and σ···π (C-H···C, $D_{C \cdots C}$ = 2.992 and 3.067 Å) bonding interactions (Figure 4a and Figure S53) and here onwards D stands for distance. On the other hand, CO_2 forms weaker σ···σ and σ···π interactions (O-C···H, $D_{C \cdots H}$ = 3.564Å, C-O···O, $D_{C \cdots O}$ = 3.265 to 3.639 Å and C-O···C, $D_{C \cdots C}$ = 3.281 Å) as shown in Figure 4b. At 273 K, β⊃CO_2 structure remains intact even with the addition of 0.5 CO_2 (β⊃1.5CO_2), which occupy two possible positions, site-I and site-IV sites (Figure 3b and Figure S54). In the case of C_2H_2 loading, a structural transformation occurs from β⊃C_2H_2 to γ⊃2.3C_2H_2 with addition of 1.3 molecules, which occupy in three positions (site-I, site-II and site-III) as shown in Figure 3a and Figure S55. The γ structure has a larger unit cell

volume and cell parameters compared to β (Table S2). When the temperature reached 195 K, β⊃1.5CO_2 underwent a phase change to γ⊃4CO_2 by addition of 2.5 CO_2. However, no phase change was observed for C_2H_2, and 1.2C_2H_2 was added to γ⊃3.5C_2H_2 which was 0.5 molecules lesser than that of γ⊃4CO_2. In the γ⊃4CO_2 structure, four CO_2 molecules occupied in five sites (site-I, site-II, site-III, site-IVa and site-IVb), which contain one additional site than the four sites (site-I, site-II, site-III and site-IV) for 3.5 C_2H_2 (Figure 4c-d and S56-57). These results reveal that CO_2 and C_2H_2 follow different pathways in terms of structural transformation and guest filling order, which leads to a reverse affinity with higher uptake for CO_2 over C_2H_2 at 195 K. With respect to host-guest or guest-guest interactions, the higher polarizability of C_2H_2 molecules resulted in the formation of strong intramolecular interactions ($D_{C \cdots H}$ = 2.676 to 3.690 Å, Figure S58). While CO_2 induces the weak intramolecular interactions ($D_{O \cdots O}$ = 3.048 to 3.763 Å, Figure S58) that indicated the possibility to fit an extra number of guest species in the pore which reveals the origin of higher uptake

Table 1. Helmholtz free energy change (ΔF), internal energy change(ΔU), and entropy change (ΔS) of the host frame for β-γ (at 273 K) and γ-δ (at 185 K) transitions induced by C_2H_4 and C_2H_6 adsorption. See, supporting information section 19 for the calculation details.

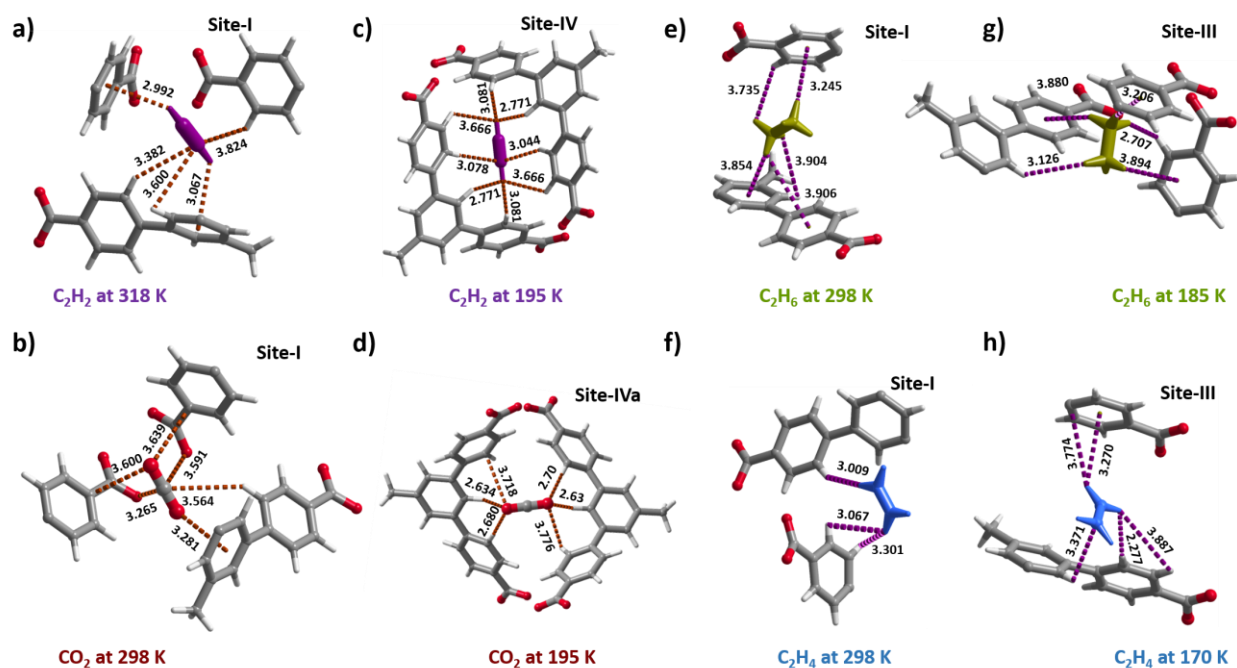|	$\Delta F_{host}^{\beta-\gamma}$ (kJ/mol-MU)	$\Delta U_{host}^{\beta-\gamma}$ (kJ/mol-MU)	$\Delta S_{host}^{\beta-\gamma}$ (kJ/mol-MU)
C_2H_4 (273 K)	1.00	1.96	3.52
C_2H_6 (273 K)	1.48	2.44	3.52
	$\Delta F_{host}^{\gamma-\delta}$ (kJ/mol-MU)	$\Delta U_{host}^{\gamma-\delta}$ (kJ/mol-MU)	$\Delta S_{host}^{\gamma-\delta}$ (kJ/mol-MU)
C_2H_4 (185 K)	3.75	2.97	-4.11
C_2H_6 (185 K)	3.71	2.95	-4.11

Figure 4. Depiction of host-guest interactions for C₂H₂, C₂H₄, C₂H₆ and CO₂ inclusion structures at various temperatures. Interactions between framework and C₂H₂ (a) or framework and CO₂ (b) at site-I. Host-guest interactions of C₂H₂ (c) or CO₂ (d) at 195 K. e and g) host-guest contacts at site-I and site-III for C₂H₆ (298 K and 185 K). Similarly, interactions sites for C₂H₆ at 298 and 170 K (f and h). Other possible host-guest and guest-guest interactions are plotted in the supporting information. All the bond distances were mentioned in the Angstrom (Å) unit.

for CO₂ at 195 K over C₂H₂. All other possible host-guest and guest-guest interactions are presented in supporting information (Figure S53 to 57).

Regarding to C₂H₆ and C₂H₄ gases, we determined the gas-adsorbed structures at three different temperatures: 298 K, 273 K, and 170/185 K[12] (Figure 3c and 3d). Both these gases follow the same trend in terms of guest filling order and occupancy. At 298 K, upon C₂H₆ or C₂H₄ dosing, β⊃empty occupy one guest species and forms β⊃C₂H₆ or β⊃C₂H₄ without altering unit cell parameters. The guest is located at site-I position in this structures, and C₂H₆ is held by both σ···σ (site-I, C-H···H, $D_{C···H}$ = 3.735 and 3.904 Å) and σ···π (site-I, C-H···C, $D_{C···C}$ = 3.245, 3.854 and 3.908 Å) interactions (Figure 4e). In contrast, C₂H₄ can only have σ···σ contacts (C-H···H, $D_{C···H}$ = 3.009, 3.067 and 3.301 Å) with the framework (Figure 4f). At 273 K, β transforms to γ by accommodating 2 guest species (γ⊃2C₂H₆ or γ⊃2C₂H₄) which are occupied at site-I and site-II (Figure S59). At cryogenic temperatures for C₂H₆ (185 K) and C₂H₄ (170 K), γ underwent phase transformation to δ, which has much larger unit cell parameters and volume (Table S2). The guest molecules at δ⊃3C₂H₆ or δ⊃3C₂H₄ are located at three sites (site-I, site-II and site-III) as shown in Figure 3c and 3d. Interestingly, C₂H₄ molecules induces strong σ···σ and σ···π interactions than C₂H₆ at cryogenic temperature. For example at site-III, C₂H₄ found to be σ and π interactions (C-H···H, $D_{C···H}$ = 2.277, 3.371, 3.774, 3.887 Å and C-H···C, $D_{C···C}$ = 3.270 Å) as shown in Figure 4h and Figure S60. C₂H₆ held with slightly weaker interactions, (C-H···H, $D_{C···H}$ = 2.707, 3.126 Å and C-H···C, $D_{C···C}$ = 3.206, 3.880 and 3.894 Å) (Figure 4g and Figure S61). This imply that at near room temperature, C₂H₆ interacts more strongly than C₂H₄, whereas at near boiling temperature, C₂H₄ binds more strongly than C₂H₆, which is correlated to experimental gas sorption. To further elucidate the mechanism behind the change in affinity and crossover sorption between C₂H₆ and C₂H₄ gases, we conducted theoretical calculations as details below.

We conducted GCMC simulations to calculate the adsorption isotherms of C₂H₄ and C₂H₆ on PCP-1 using optimized atomistic models. We also attempted to explain the gate pressure inversion phenomenon using existing methods for free energy analysis (for more information about the calculation methods, see the supporting information Figures S62-65 and Table S6-8). Figures 5, S63, S64, and Table 1 present the results of adsorption simulations and free energy analysis for the β−γ transition at 273 K (Figures 5a,b and S63) and γ−δ transition at 185 K (Figures 5c,d and S64). The fictitious adsorption isotherms of C₂H₄ on "immobilized" β, γ, and δ structures obtained from GCMC simulations, $N_{C2H4}^{β}$, $N_{C2H4}^{γ}$, and $N_{C2H4}^{δ}$, show good agreement with the plateau regions of measured C₂H₄ adsorption isotherms before and after gated adsorption (Figure 5a for 273 K and 5c for 185 K). Similarly, the fictitious adsorption isotherms of C₂H₆, $N_{C2H6}^{β}$, $N_{C2H6}^{γ}$, and $N_{C2H6}^{δ}$ show good agreement with the measured C₂H₆ adsorption isotherms before and after gated adsorption (Figure 5b for 273 K and 5d for 185 K). It is interesting to note that $\Delta S_{host}^{γ-δ}$ is observed to be negative. At

Table 2. s-f (U_{sf}) and f-f (U_{ff}) interactions at each site in the γ structure and their summed values

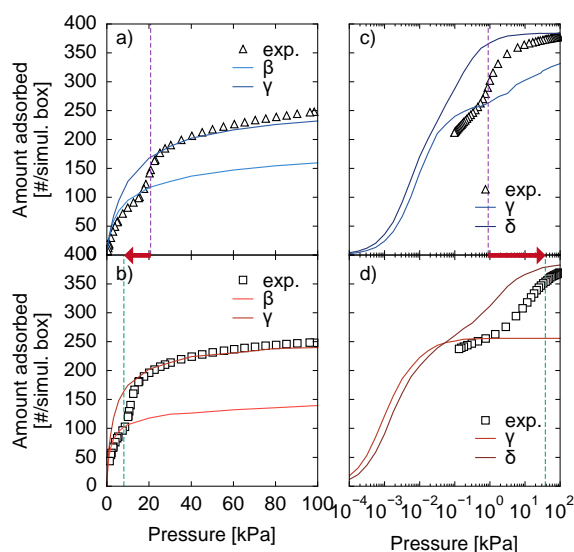|	U_{sf} (site I) (kJ/mol)	U_{sf} (site II) (kJ/mol)	U_{sf} (site III) (kJ/mol)	U_{sf} (all) (kJ)
C₂H₄	36.5	42.9	33.2	112.7
C₂H₆	35.4	44.8	33.9	114.1
	U_{ff} (site I-II) (kJ/mol)	U_{ff} (site II-III) (kJ/mol)	U_{ff} (site I-III) (kJ/mol)	U_{ff} (all) (kJ)
C₂H₄	0.65	2.81	6.84	10.30
C₂H₆	1.27	2.13	4.82	8.22

5

Figure 5. Adsorption simulation results of (a) C_2H_4 and (b) C_2H_6 on the structures β and γ at 273 K and (c) C_2H_4 and (d) C_2H_6 on the structures γ and δ at 185 K. Empty black triangles (a and c) and squares (b and d) represents the experimental sorption for C_2H_4 and C_2H_6, respectively. Dark and light blue (a and c) lines represent the fictitious adsorption isotherms of C_2H_4. Similarly, dark and light red lines for C_2H_6 sorption. Purple and green dashed lines represent the referenced and predicted gate pressures, respectively.

first glance, it may seem unnatural that $\Delta S_{host}^{\gamma-\delta}$ should be negative, as the structural deformation from γ to δ is accompanied by volume expansion, as shown in Table S5. However, a closer inspection of the lattice parameters reveals that while the lattice constant b increases from γ to δ, a and c decrease (Table S5). Additionally, the number of adsorbed molecules in the δ structure is 1.5 times larger than in the γ structure, despite the small increase in volume. This suggests that the organic ligands in the framework are pushed into the pore when in the adsorption state. These results suggest that $\Delta S_{host}^{\gamma-\delta}$ is negative due to the reduction in the number of possible states of the organic ligands. The theoretical gate pressures estimated from thermodynamic analysis method, are summarized in Table S6. As seen in the Table S7, the free energy analysis based on gated adsorption theory shows that $P_{g.C2H6}$ is less than $P_{g.C2H4}$ for the β−γ transition at 273 K, while, $P_{g.C2H4}$ is less than $P_{g.C2H6}$ for the γ−δ transition at 185 K. These results confirm that the atomistic model is able to reproduce the gate pressure inversion phenomenon, and the thermodynamic analysis method of gated adsorption[14] has successfully explained the crossover sorption behaviour theoretically.

When comparing the fictitious adsorption isotherm of C_2H_4 and C_2H_6 on the δ structure, there is a distinct difference in the way the adsorption amount increases as pressure increases (Figure S65). Therefore, the isosteric heat of adsorption (Q_{st}) for the δ structures of C_2H_4 and C_2H_6 were further calculated (Figure 6a, see supporting information section 19 for the calculation details). In the adsorption of C_2H_4, Q_{st} increased significantly after the adsorption amount exceeded 200 for the simulated cell, indicating that the interaction among adsorbed molecules becomes stronger as the number of adsorbed molecules increases. As shown by in situ SCXRD results, PCP-1 exhibits a two-step structural transition, i.e. β−γ and γ−δ transitions, upon C_2H_4 and C_2H_6 adsorption. The number of crystallographically independent adsorption sites increases one by one during this transition. Before the transition, the β structure has eight adsorption sites (site I) per unit cell. When the structure transitions to the γ structure, another pore is created, resulting in eight new adsorption sites (site II). Furthermore, when the structure changes to the δ
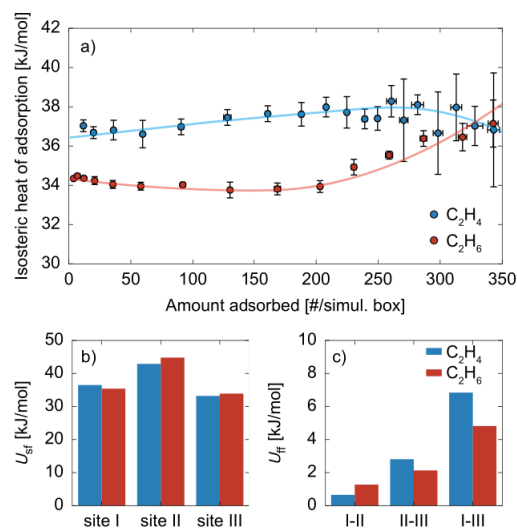

Figure 6. (a) The isosteric heat of adsorption (Q_{st}) for the δ phase of C_2H_4 and C_2H_6, where lines are guides for the eye. (b) The calculated solid-fluid (s-f) interaction between the adsorbent and adsorbed guest species. (c) The calculated fluid-fluid (f-f) interaction (fluid-fluid: f-f). In (b) and (c), the blue and red bars represent the calculation results for C_2H_4 and C_2H_6, respectively.

structure, the pore space corresponding to site I expands, and a new adsorption site (site III) is created in the same pore (Figure 3c and 3d). To identify the factor responsible for the increase in the Q_{st} of C_2H_4 observed in Figure 6a, we focused on the three adsorption sites (site I, site II, and site III) of the δ structure, and calculated the interaction between the adsorbent and adsorbed molecules (solid-fluid: s-f), and the interaction between adsorbed molecules (fluid-fluid: f-f) (Figure 6b, c and Table 2; See, supporting information section 19 for the calculation details). The s-f interaction showed little difference between C_2H_4 and C_2H_6 at any adsorption site, but the overall value was slightly larger for C_2H_6. On the other hand, for the f-f interaction, the difference between C_2H_4 and C_2H_6 was substantial, particularly between sites I-III, with C_2H_4 showing a stronger interaction. To examine the f-f interaction between sites I-III, we calculated the molar density in the pore in the δ structure. It was found that the molar density in the pore was similar to that of the bulk solid for both C_2H_4 and C_2H_6 (Table S8), suggesting that the interactions between adsorbed molecules in the γ-structure site I-III are comparable to those in the bulk solid. In other words, in the δ structure, the adsorbed molecules are packed at the same density as the bulk solid, and C_2H_4, which is a planar molecule, can form a more stable adsorption phase at this time. Therefore, in the γ−δ transition, C_2H_4 could be adsorbed at lower pressure than C_2H_6, reflecting the difference in stability between the solid state C_2H_4 and C_2H_6. On the other hand, in structures β and γ, the adsorbed molecules are finely delimited by the host framework, and the adsorption phenomenon depends only on the dispersion force with the wall surface. In fact, adsorption energy for C_2H_4 and C_2H_6 in the γ structure were estimated as 45.1 and 46.6 kJ/mol, respectively, indicating that C_2H_6 shows the dispersion force with the wall surface likely due to the larger molecular weight. Therefore, these calculations suggest that the inversion of gate pressure in PCP-1 is caused by a subtle balance between s-f and f-f interactions at the each adsorbed phases.

Conclusions

In summary, herein we reported a first observation of soft porous coordination networks, PCP-1 and PCP-2 that exhibits crossover sorption with reverse affinity and uptake capacity for both C_2H_2/CO_2 and C_2H_6/C_2H_4. This phenomenon was verified by both sorption isotherm and isobar measurements at different temperature

ranges. In-situ single crystal X-ray diffraction measurements and DFT calculations were used to elucidate the mechanisms. Upon inspecting the guest inclusion structures of C_2H_2 and CO_2, it was revealed that at near room temperature, C_2H_2 has a tendency to interact strongly with the framework, resulting in gate opening, whereas CO_2 does not. However, at cryogenic temperatures, CO_2 has an additional binding site, which increases its uptake capacity over that of C_2H_2. DFT calculations demonstrated that with regards to C_2H_6/C_2H_4, host-guest interactions favored C_2H_6 at room temperature, whereas guest-guest interactions dominated for C_2H_4 at cryogenic temperatures, resulting in a reversal of affinity. Additionally, this study showed that the crossover temperature could be adjusted through framework functionalization, specifically by switching from methyl to methoxy groups for C_2H_2/CO_2 or C_2H_6/C_2H_4 gases (Table S4). Our findings could lead to possibilities for functionalization with other groups, for example, amino, fluorine, and sulfur derivatives, which have the potential to modify the crossover temperature and enhance selectivity and separation performance. Additionally, our findings suggest that a single sorbent displaying a crossover phenomenon can separate gas1 from gas2 and gas2 from gas1 by simply adjusting the temperature, potentially obviating the need for multiple separate sorbents in the separation processes. In summary, this study provides insights into the mechanism of flexible sorbents when guest species are included and can assist in designing new sorbents for specific applications.

Conflict of interest

The authors declare no conflict of interest.

Keywords: porous coordination polymer · flexibility · crossover sorption · C_2H_2/CO_2 and C_2H_6/C_2H_4 sorption · in-situ characterization

References

[1] a) M. E. Davis, *Nature* **2002**, *417*, 813; b) Y. Chai, X. Han, W. Li, S. Liu, S. Yao, C. Wang, W. Shi, I. da-Silva, P. Manuel, Y. Cheng, L. D. Daemen, A. J. Ramirez-Cuesta, C. C. Tang, L. Jiang, S. Yang, N. Guan, L. Li, *Science* **2020**, *368*, 1002.

[2] a) S. Kitagawa, R. Kitaura, S. Noro, *Angew. Chem. Int. Ed.* **2004**, *43*, 2334-2375; b) S. R. Batten, S. M. Neville, D. R. Turner, *Coordination polymers: design, analysis and application introduction*, RSC Publishing, Cambridge, UK, **2009**.

[3] a) L. R. MacGillivray, C. M. Lukehart, *Metal-Organic Framework Materials*, Wiley, **2014**; b) M. Schroder, in *Functional Metal-Organic Frameworks: Gas Storage, Separation and Catalysis*, Topics in Current Chemistry **2010**, 1-262; c) M. Ding, R. W. Flaig, H.-L. Jiang, O. M. Yaghi, *Chem. Soc. Rev.* **2019**, *48*, 2783-2828.

[4] a) S. Kitagawa, M. Kondo, *Bull. Chem. Soc. Jpn* **1998**, *71*, 1739-1753; b) S. Horike, S. Shimomura, S. Kitagawa, *Nat. Chem.* **2009**, *1*, 695-704.

[5] a) A. Schneemann, V. Bon, I. Schwedler, I. Senkovska, S. Kaskel, R. A. Fischer, *Chem. Soc. Rev.* **2014**, *43*, 6062-6096; b) S. K. Elsaidi, M. H. Mohamed, D. Banerjee, P. K. Thallapally, *Coord. Chem. Rev.* **2018**, *358*, 125-152; c) G. Ferey, C. Serre, *Chem. Soc. Rev.* **2009**, *38*, 1380-1399; d)

R. E. Morris, L. Brammer, *Chem. Soc. Rev.* **2017**, *46*, 5444-5462; e) M. Shivanna, Q.-Y. Yang, A. Bajpai, E. Patyk-Kazmierczak, M. J. Zaworotko, *Nat. Commun.* **2018**, *9*, 3080.

[6] a) S. Krause, N. Hosono, S. Kitagawa, *Angew. Chem. Int. Ed.* **2020**, *59*, 15325-15341; b) M. Shivanna, Q. Y. Yang, A. Bajpai, S. Sen, N. Hosono, S. Kusaka, T. Pham, K. A. Forrest, B. Space, S. Kitagawa, M. J. Zaworotko, *Sci. Adv.* **2018**, *4*, eaaq1636; c) M. Shivanna, K. I. Otake, B. Q. Song, L. M. van Wyk, Q. Y. Yang, N. Kumar, W. K. Feldmann, T. Pham, S. Suepaul, B. Space, L. J. Barbour, S. Kitagawa, M. J. Zaworotko, *Angew. Chem. Int. Ed.* **2021**, *60*, 20383-20390.

[7] a) H. Zeng, M. Xie, T. Wang, R.-J. Wei, X.-J. Xie, Y. Zhao, W. Lu, D. Li, *Nature* **2021**, *595*, 542-548; b) G. L. Smith, J. E. Eyley, X. Han, X. Zhang, J. Li, N. M. Jacques, H. G. W. Godfrey, S. P. Argent, L. J. McCormick McPherson, S. J. Teat, Y. Cheng, M. D. Frogley, G. Cinque, S. J. Day, C. C. Tang, T. L. Easun, S. Rudic, A. J. Ramirez-Cuesta, S. Yang, M. Schroder, *Nat. Mater.* **2019**, *18*, 1358-1365

[8] a) C. Gu, N. Hosono, J.-J. Zheng, Y. Sato, S. Kusaka, S. Sakaki, S. Kitagawa, *Science* **2019**, *363*, 387-391; b) Y. Su, K.-i. Otake, J.-J. Zheng, S. Horike, S. Kitagawa, C. Gu, *Nature* **2022**, *611*, 289-294; c) M. H. Yu, B. Space, D. Franz, W. Zhou, C. He, L. Li, R. Krishna, Z. Chang, W. Li, T. L. Hu, X. H. Bu, *J. Am. Chem. Soc.* **2019**, *141*, 17703-17712.

[9] M. L. Foo, R. Matsuda, Y. Hijikata, R. Krishna, H. Sato, S. Horike, A. Hori, J. Duan, Y. Sato, Y. Kubota, M. Takata, S. Kitagawa, *J. Am. Chem. Soc.* **2016**, *138*, 3022-3030.

[10] a) B. Chen, Q. Dong, X. Zhang, S. Liu, R.-B. Lin, Y. Guo, Y. Ma, A. Yonezu, R. Krishna, G. Liu, J. Duan, R. Matsuda, W. Jin, *Angew. Chem. Int. Ed.* **2020**, *59*, 22756–22762; b) B. Q. Song, Q. Y. Yang, S. Q. Wang, M. Vandichel, A. Kumar, C. Crowley, N. Kumar, C. H. Deng, V. GasconPerez, M. Lusi, H. Wu, W. Zhou, M. J. Zaworotko, *J. Am. Chem. Soc.* **2020**, *142*, 6896-6901.

[11] R.-B. Lin, H. Wu, L. Li, X.-L. Tang, Z. Li, J. Gao, H. Cui, W. Zhou, B. Chen, *J. Am. Chem. Soc.* **2018**, *140*, 12940-12946.

[12] Crystallographic data in CIF format have been deposited in the Cambridge Crystallographic Data Centre (CCDC) under deposition numbers 2267987 (PCP1-as synthesized), 2267967 (PCP1-activated), 2267997 (PCP1@C2H6 298K), 2267996 (PCP1@C2H6 273K), 2267995 (PCP1@C2H6 185K), 2267994 (PCP1@C2H4 298K), 2267966 (PCP1@C2H4 273K), 2267993 (PCP1@C2H4 170K), 2267990 (PCP1@C2H2 318K), 2267965 (PCP1@C2H2 273K), 2267989 (PCP1@C2H2 195K), 2267992 (PCP1@CO2 298K), 2269678 (PCP1@CO2 273K), 2267991 (PCP1@CO2 195K), 2267988 (PCP2-as synthesized), and 2268301 (PCP2-activated).

[13] a) X. Jiang, Y. Wang, J.-W. Cao, Z.-M. Ye, T. Zhang, D.-X. Liu, K.-L. Li, R. Yang, T. Wang, Q.-Y. Zhang, K.-J. Chen, *Chem. Eur. J.* **2021**, *27*, 12753-12757; b) K. J. Chen, D. G. Madden, S. Mukherjee, T. Pham, K. A. Forrest, A. Kumar, B. Space, J. Kong, Q. Y. Zhang, M. J. Zaworotko, *Science* **2019**, *366*, 241-246; c) P.-Q. Liao, A.-X. Zhu, W.-X. Zhang, J.-P. Zhang, X.-M. Chen, *Nat. Commun.* **2015**, *6*, 6350; d) S.-M. Wang, F. Wang, Y.-L. Dong, M. Shivanna, Q. Dong, X.-T. Mu, J. Duan, Q. Yang, M. J. Zaworotko, Q.-Y. Yang, *Separation and Purification Technology* **2021**, *276*, 119385; e) C. Gücüyener, J. van den Bergh, J. Gascon, F. Kapteijn, *J. Am. Chem. Soc* **2010**, *132*, 17704-17706.

[14] F.-X. Coudert, M. Jeffroy, A. H. Fuchs, A. Boutin, C. Mellot-Draznieks, *J. Am. Chem. Soc.* **2008**, *130*, 14294-14302.

Entry for the Table of Contents
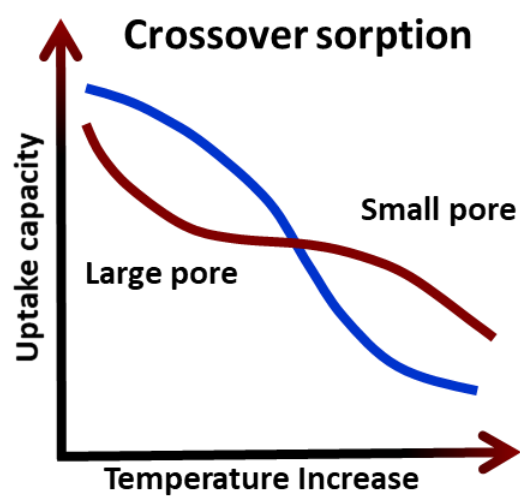
Flexible coordination networks exhibit crossover sorption with change in affinity and uptake capacity on varying the temperature. The coordination networks show reverse affinity and uptake capacity for both C_2H_2/CO_2 and C_2H_6/C_2H_4. This phenomenon was verified by both sorption isotherm and isobar measurements at different temperature ranges. In situ single-crystal X-ray diffraction and DFT calculations were used to elucidate the mechanisms.

Twitter account: @KitagawaGroup and @iCeMS_KU